Global Distribution and Associated Synoptic Climatology of Very Extreme Sea States (VESS)

V. J. Cardone[1], A. T. Cox[1], M. A. Morrone[1],
and Val R. Swail[2]

[1]Oceanweather Inc
Cos Cob, CT, USA

[2]Environment Canada
Toronto, Ontario, Canada

1. INTRODUCTION

Very extreme sea states (VESS) are of great interest to designers of vessels and offshore and coastal infrastructure and users of high-seas operational wave forecasts. While there is no generally agreed precise definition of a VESS threshold in terms of significant wave height (HS), ~ 14 m +/- 1 m seems appropriate as this magnitude of sea state is rarely sampled in the in-situ network of buoy and platform mounted sensors, which admittedly lie mainly along the continental margins, and is comparable to design level sea states (return period of ~50-100 years) in most active oceanic regions of offshore resource production. Indicative of this interest is the recently established WMO-IOC Joint Technical Commission for Oceanography and Marine Meteorology (JCOMM) initiative to establish a community database of VESS occurrences (Soares and Swail, 2006). The recent EU MaxWave project (Rosenthal and Lehner, 2008) and the CREST Joint Industry Project (Buchner *et al*, 2011) have addressed the incidence and cause(s) (e.g Garrett and Gemmrich, 2009; Waseda *et al*., 2009) of occurrences of extreme individual crest heights and wave heights the most impactful of which will tend to occur within VESS.

VESS and the storms in which they occur have also become of great interest to the wave modeling community. Third-generation spectral ocean wave models perform very well over most of the dynamic range of naturally occurring wave regimes but there has been reported a tendency for reduced skill and some negative bias in specification of very extreme sea states (e.g. Cardone *et al*., 1996) though that tendency appears to be alleviated when the atmospheric forcing is carefully prescribed (e.g. Cardone and Cox, 2011). As fourth generation wave models are developed and introduced, the improvements in physics and/or numerics of such models should be tested against tropical and extratropical storms that generate VESS. Specification of atmospheric forcing in such storms of sufficient accuracy that wind field errors do not mask model physics effects has been difficult in the past due to the sparseness of open-ocean in-situ marine wind measurements, but within the past two decades great advances in monitoring the time and space evolution of surface wind fields of hurricanes by airborne flight level and surface wind sensors (e.g. Powell *et al*. 2009), and of extratropical cyclones (ETC) by satellite mounted passive and active microwave marine surface wind sensors (e.g. Cardone *et al*., 2004) have made accurate wind field specifications possible in all NH and SH mid-latitude regions affected.

This study basically follows up our preliminary study reported by Cardone *et al.*, 2009 (henceforth C09) on the detection of VESS by satellite radar altimeters. Here, we utilize the newly released comprehensive GlobWave database (1985-present) of global satellite altimeter HS and wind speed (WS) estimates (Ash *et al*., 2011). Relative to the altimeter databases referred to in C09, GlobWave includes all missions flown since 1985, and employed greater quality control (QC) of the data streams, and homogenized the retrieval algorithms that transform radar return to HS. Whereas in C09 a labor-intensive QC procedure had to be followed to extract VESS occurrences from the altimeter data streams, in this study we applied a simple objective algorithm to find distinct altimeter peaks of HS > 12 m (below the stated 14 m VESS

threshold) along basin-specific orbit segments, where the basins are defined conventionally as North Atlantic Ocean (NAO), North Pacific Ocean (NPO), South Atlantic Ocean (SAO), South Pacific Ocean (SPO), South Indian Ocean (SIO). Minimal subsequent QC was required. The population of over 5000 peaks identified was then distilled to a unique set of storms. Perhaps surprisingly, the storms with the highest peaks of HS were found in the NAO and NPO where several occurrences of HS ~ 20 m were found to be associated with rapidly intensifying mid-latitude ETC within which peak surface wind speeds (equivalent neutral 30-minute average at 10-m elevation) attained super-Beaufort (> 64 knots average peak) wind speeds at the time of maximum intensity. In the Southern Oceans, only the Southern Indian Ocean SIO approaches the NH basins in absolute maximum sea states with a population peak HS of ~ 17.5 m. Normalized by the sizes of the basins it appears that the NAO has by a wide margin the highest frequency of occurrence of VESS ETC. Only a handful of VESS detected were found to be associated with tropical cyclones, a result that we believe is associated mainly with the small scale of the area of peak sea states in such systems making detection of the inner core of tropical cyclones by satellite mounted nadir pointing altimeters rare. Rain contamination/attenuation of the altimeter radar signal may also play a role in the small number of tropical cyclones detected. Therefore, almost all of the peaks described in this study are associated with strong ETC the most intense of which have been dubbed "winter hurricanes" (e.g. Von Ahn *et al*., 2006).

This study also utilized a recent continuous atmospheric reanalysis product (National Centers for Environmental Projection (NCEP), National Oceanic and Atmospheric Administration (NOAA) Climate Forecast System Reanalysis (CFSR)) and, in some cases, the products of our more detailed storm-by-storm reanalysis, to help define the principal synoptic characteristics of the ETC associated with VESS, summarization of which leads to a proposed simple conceptual model of VESS storm evolution. Finally, we report the results of a high resolution NAO basin 3G model wave hindcast of the first half of February, 2007, during which the two highest ranked NAO VESS storms were detected. Atmospheric forcing for this hindcast is aided by greatly by QuikSCAT monitoring. Validation of the hindcast against orbit segments that sampled VESS in these two events illustrates the potential of the GlobWave data to assess model performance in such extreme storms.

2. ALTIMETER DATA SET

GlobWave provides a new, homogenized, quality controlled, single point of access database containing virtually the entire record of satellite altimeter HS and WS measurements. Table 1 lists all the missions included in GlobWave, this study only applied data from 1991 onward. Figure 1 shows that since 1991, the number of simultaneous missions has ranged from just one in 1991 to five during much of 2002-2005. The database is described in a general way in the Wave Data Handbook for GlobWave (Ash *et al*., 2011). More details on the quality control procedures and calibration of the data streams from the various missions are given by Queffeulou and Croize-Fillon (2010) (QC2010). They describe a series of mission dependent quality tests that were applied to produce a set of quality flags for each estimate, followed by additional filters applied to data near coasts, in so-called sigma0 blooms (Thibault *et al*., 2007), and to filter excessive changes between successive 1Hz estimates along track. Individual estimates indicated by land and sea masks to be contaminated by sea ice or land were also eliminated. QC2010 also revisited the critical issue of calibration of the altimeter radar return - HS algorithm and updated the regressions for each mission based on comparisons of the altimeter measurements against worldwide buoy wave measurements. The standard error of the HS estimates overall is considered to range from about 0.8 m at HS ~ 4 m to about 1.7 m at HS ~12 m. Except for ERS1, and in the data range of most of the altimeter-buoy comparisons (HS < ~ 8 m) the mean differences between the recalibrated altimeter HS and the buoy HS comparisons data sets are within +/- 0.25 m and vary by mission, but there remain issues with regard to the extent to which the buoy data sets themselves can be considered to be unbiased. A JCOMM buoy wave measurement inter-comparison program is currently investigating this issue with a dedicated field program, see: (http://www.jcomm.info/index.php?option=com_content&task=view&id=62).

An analogous effort to QC and homogenize the calibration of Ku band sigma0 derived WS is also described by QC2010 and that work appears to have led to the imparting of a wider dynamic range of altimeter Ku band wind speeds in the GlobWave database than in previously processed satellite altimeter WS datasets.

For this study, GlobWave data were acquired for the period 8/1/1991 to 3/3/2010. The time periods included for the various altimeters are as follows: ERS1 8/1/1991 – 6/2/1996; ERS2 5/15/1995 – 5/11/2009; ENVISAT: 9/27/2002 to 12/7/2009; TOPEX: 9/25/1992 – 10/8/2005; JASON-1: 1/15/2002 – 3/3/2010; JASON-2 7/4/2008 – 3/3/2010 GEOSAT FO: 1/7/2000- 9/7/2008. The native format of the data is netCDF time sorted, all missions combined. For the study, the data set was processed to separate monthly files sorted by altimeter.

Table 1.
Altimeter missions included in GlobWave database (from Globwave Wave Data Handbook)

Satellite	Altimeter	Agency	Dates	Altitude	Inclination	Repeat
Geosat		US Navy	1985 - 1989	800 km	108°	17 days
ERS-1	RA	ESA	1991 - 1996	785 km	98.5°	35 days (3 days, 168 days)
TOPEX/Poseidon	TOPEX and Poseidon-1	NASA / CNES	1992 - 2005	1336 km	66°	10 days
ERS-2	RA	ESA	1995 - 2003	785 km	98.5°	35 days
GFO	GFO-RA	US Navy / NOAA	2000 - 2008	800 km	108°	17 days
Jason-1	Poseidon-2	CNES / NASA	2001 -	1336 km	66°	10 days
Envisat	RA-2	ESA	2002 -	800 km	98.5°	35 days
Jason-2	Poseidon-3	CNES / NASA / Eumetsat / NOAA	2008 -	1336 km	66°	10 days

3. VESS DETECTION

As in C09, the main objectives of the analysis were to identify all basin specific orbit segments with a peak HS > 12m in the 1Hz data stream, identify and remove any remaining spurious spikes from this data set, summarize the spatial distribution and range of those occurrences by mission, distill the occurrences into parent storms and extract associated meteorological characteristics of the parent storms from global reanalysis data products and remotely sensed surface marine wind data. In C09, the first two steps were done basically by hand in a very labor intensive process because of the large number of spurious spikes and other errors in the altimeter data streams. GlobWave is a much "cleaner" file when only the data samples flagged as "probably good measurement" are retained as was done here.

Orbit segment peaks were first identified objectively using a "peak-finder" algorithm that follows the orbital data flow and seeks the absolute maximum of HS in the 1Hz stream that is unique with respect to a specified along track distance window (set to 400 nm) and time window (set to 5 minutes). For each so identified orbit segment, a 15-minute orbital slice centered on the peak was plotted as shown in Figure 2, which also for reference displays the closest hourly analysis of wind speed and sea level pressure in a 60 degree latitude-longitude box centered on the orbit. The source of the wind field and pressure fields is the new CFSR reanalysis (Saha *et al*., 2010). Of the 5320 orbital segments found in this way with peak HS > 12 m, further QC led to the rejection of only 64 (~ 1.2%) as representing either spurious spikes or ambiguous cases near an ice edge.

The distribution of the final population of 5256 peaks by altimeter and basin, along with relative percentages, are provided by Tables 2 and 3, respectively. C09 reported only 260 peaks, which is a factor of ~20 fewer than found in GlobWave. This difference can be explained by several factors. First, the scan here is based on altimeter data scanned at the intrinsic sampling rate, whereas in C09 the altimeter data were spatially bin-averaged before scanning. Second, C09 examined only three missions (TOPEX, JASON-1, ENVISAT) comprising about 300 months of data compared to nearly 700 months of data in the seven missions in GlobWave. Third, whereas in C09 the ENVISAT record was found curiously to contain virtually no peaks of HS > 12 m, the GlobWave database for ENVISAT now contains 661 cases. Finally, the recalibration of all instruments and algorithms has tended to increase the retrieved HS and therefore move many prior estimates that were just below 12 m to just beyond the 12 m threshold. It is seen in Table 2 that SIO contains the most cases at 32% and the SAO the least number of peaks at 7%. The NAO includes 26% of the cases, which is remarkable considering that the NAO basin is about a factor of 3 smaller in extent at mid-latitudes than the SIO. Table 3 shows the distribution of peaks by basin and HS ranges (HS > 12 m, HS > 14 m, HS > 16 m). For the latter two classes, the NAO now leads the occurrences on an absolute basis over all other basins. The four panel plot in Figure 3 shows the global distribution of peaks from all altimeters combined and for three ranges of VESS while Figure 4 shows the distribution of VESS by altimeter. A labor-intensive search for cases associated with tropical cyclones found 147 peaks > 12 m (less than 3% of the data). Only five of these samples had HS > 16 m. Certainly, VESS have been documented to occur in tropical cyclones worldwide in the in-situ and platform measurement record (e.g. Jensen *et al*., 2006; Cardone and Cox, 2011, Chao and Tolman, 2010) but it is difficult for an altimeter to "see" an extreme sea state in a tropical cyclone mainly because the small scale of the area of peak sea states in such systems makes the chance scanning of the inner core of tropical cyclones by satellite mounted nadir pointing altimeters very rare. Also, heavy convective rain in the inner core would tend to cause the radar beam to fail to properly sample the wavy surface.

Table 2.
GlobWave distribution of basin orbit-segment peaks of HS > 12 m along (counts and relative percentage occurrence) sorted by altimeter mission and basin

Satellite	NATL	%NATL	NPAC	%NPAC	SATL	%SATL	SPAC	%SPAC	SIND	%SIND	TOTAL	%TOTAL
ERS1	130	9.67	83	8.37	41	11.71	85	9.54	167	9.95	506	9.63
ERS2	246	18.29	180	18.15	39	11.14	81	9.09	162	9.65	708	13.47
TOPEX	404	30.04	301	30.34	97	27.71	290	32.55	495	29.50	1587	30.19
ENVISAT	146	10.86	106	10.69	53	15.14	117	13.13	239	14.24	661	12.58
GFO	160	11.90	165	16.63	59	16.86	138	15.49	299	17.82	821	15.62
JASON1	223	16.58	144	14.52	54	15.43	154	17.28	273	16.27	848	16.13
JASON2	36	2.68	13	1.31	7	2.00	26	2.92	43	2.56	125	2.38
TOTAL	1345	25.59	992	18.87	350	6.66	891	16.95	1678	31.93	5256	100.00

Table 3.
Distribution of orbit segment peaks (counts and relative percentage occurrence) sorted by basin for indicated HS thresholds.

HS	NATL	%NATL	NPAC	%NPAC	SATL	%SATL	SPAC	%SPAC	SIND	%SIND	TOTAL	%TOTAL
>16 m	65	4.83	34	3.43	6	1.71	15	1.68	65	3.87	185	3.52
>14 m	310	23.05	222	22.38	58	16.57	138	15.49	318	18.95	1046	19.90
>12 m	1345	25.59	992	18.87	350	6.66	891	16.95	1678	31.93	5256	100.00
Maximum HS (m)	**20.24**		**20.63**		**16.57**		**17.51**		**18.84**			

4. VESS STORMS

The distillation of the individual orbital peaks to a population of high ranked associated ETC was a two-step process. First, to keep this part of the study tractable for now, the threshold of peak HS was raised to HS > 16m, which as indicated in Table 3 includes 185 cases. Second, the 185 candidate orbits were distilled to a unique set of storms by scanning the orbital plots together with associated weather map sequences, thereby identifying the often several orbits that transected the same storm at different locations and different times in its life-cycle. To aid this distillation, both the CFSR wind fields and a

preliminary deep water global wave hindcast (Cox *et al*., 2011) on a 70-km grid forced by CFSR winds were color contoured and displayed together with each of the 185 orbital segments containing a peak HS > 16 m. Figure 5 shows a rather typical example of such a plot for the top ranked NAO storm of February 9, 2007 also discussed and hindcast in C09. Note that the CFSR wave hindcast is quite skillful overall with only the part of the storm very near the core of the peak under-predicted by a few meters. Figure 6 is a corresponding sample of a statistical comparison of the hindcast and the altimeter data for this orbit, which indicates for hindcast versus altimeter HS a correlation coefficient of 0.98, scatter index of 0.15 and bias of -.05 m. Figure 5 also shows for the altimeter data, both the 1 Hz estimates of HS along the orbit and (as larger crosses) median filtered values derived from 1 Hz estimates binned within 50-km along orbit segments. Strengths and deficiencies of the CFSR as a wave model forcing data set are discussed in more detail by Cox *et al*. (2011). Here we note only that for the storm peaks along the 185 orbit segments the CFSR driven hindcast peaks are biased low by 2.3 m with respect to the 1 Hz peaks above 16 m and 1.4 m low with respect to the peak of the median filtered altimeter estimates. We consider this a remarkable achievement and suggests that the CFSR is markedly more accurate than previous efforts at least within the historical period of these storms (late 1992 to early 2010).

The population of 185 peaks was ultimately distilled to a population of 120 individual storms consisting of 116 extratropical storms and 4 tropical cyclones. Table 4 gives the date, location and peak HS of the altimeter storm peaks in these storms and some associated storm properties as taken from CFSR. We had expected that the detection rate of these VESS storms would increase over time since the number of altimeter missions generally increased from an average of 2.25 missions in space at any given time during the decade of the 1990s (or the period 1992-1999 to be more precise) to an average of 4.63 missions during the period 2002 – 2009. Despite this nearly doubling of altimeter sampling, we find about the same global frequency of VESS storms per year in both periods at about 5 storms/year.

Table 4.
Orbit-segment peaks (at intrinsic sampling rate) of HS > 16 m and associated storm properties from CFSR

Full Stormname	Latitude	Longitude	Satellite	Altimeter Peak Hs (m)	Bearing	Range (degrees)	Lowest CFSR SLP (mb)	CFSR Po / Delta T (mb/day)	CFSR Max Ws (kts)
199903180526	45.61	183.4	TOPEX	20.63	SSW	6.5	949	28	73
200702101108	48.14	327.35	GFO	20.24	SW	3	963	24	75
199903212109	51.14	176.81	TOPEX	19.5	SSE	2.5	937	52	73
200602031141	40.79	178.3	JASON1	19.39	SSW	6	959	44	75
200702092131	48.63	341.15	JASON1	19.15	SSE	3	951	36	77
199502020709	50.75	326.56	TOPEX	19.1	SSE	5	935	50	71
200610090425	-53.59	110.36	GFO	18.84	NNE	3	939	42	71
200501171517	57.13	328.43	TOPEX	18.78	SW	6.5	945	32	69
200705130900	-39.71	57.04	JASON1	18.71	NW	8	943	28	63
200002081151	57.73	336.52	GFO	18.64	SW	2.5	953	42	75
199401072219	58.03	316.7	TOPEX	18.57	NW	1.5	965	6	75
200302120845	48.25	319.5	TOPEX	18.27	SSE	5	949	46	71
200809020748	-52.49	21.86	ENVISAT	18.18	NNE	5	939	26	65
200611260524	46.63	333.03	GFO	18.16	SSW	3	947	38	73
200703102252	58.92	334.57	JASON1	18.13	SE	3	945	38	71
200802041046	37.2	162.01	ENVISAT	18.09	SW	3.5	955	36	71
199301102123	60.71	352.64	TOPEX	18.05	SE	4	913	64	89
200202012211	59.84	350.59	GFO	18.01	SE	3.5	931	60	75
200512232252	42.37	174.8	ENVISAT	18	SSE	7.5	943	32	63
199410140925	-56.09	100.48	TOPEX	17.83	NNE	6	933	36	59
199312042352	-51.5	116.3	TOPEX	17.83	NW	8	943	38	61
200604041651	-55.45	89.9	ENVISAT	17.81	NE	6	927	44	67
200409221815	27.61	311.45	JASON1	17.71	TROPICAL				
200511051706	-53.93	85.48	ENVISAT	17.66	NW	4	935	24	57
200406231814	-57.27	20.6	TOPEX	17.66	NE	2.5	921	32	61
200207311229	-56.22	72.19	TOPEX	17.66	NNE	6	935	32	67
200408211606	-55.72	58.68	GFO	17.58	NW	3.5	957	24	63
200909211703	-50.52	84.56	ENVISAT	17.55	NW	4.5	943	34	69
199501080603	40.18	184.98	TOPEX	17.52	S	4	961	30	65
199601051812	42.51	330.61	TOPEX	17.51	SW	6	947	34	67
200306010841	-56.87	174.25	GFO	17.51	NE	3	935	36	71
200508191748	-44.89	63.96	JASON1	17.48	NW	5.25	955	24	69
200212041450	-50.73	19.28	TOPEX	17.45	NW	10	943	36	59
200003161836	-53.63	90.14	GFO	17.42	NW	7	951	30	57
199401181846	59.26	333.76	TOPEX	17.41	SSE	4.5	951	36	63

199408141934	-60.55	221.3	TOPEX	17.41	NW	6.5	931	30	63
199912021545	44.87	187.27	TOPEX	17.35	SW	6	961	40	75
199909120101	-54.47	233.84	TOPEX	17.35	NNW	6	935	36	61
200901160618	54.86	316.85	JASON1	17.31	SE	3	947	32	75
199409041923	-53.6	68.13	TOPEX	17.31	NW	7.5	943	28	61
199210132214	-51.96	90.04	TOPEX	17.31	NW	9	945	19 (13 hr)	57
200003211125	36.13	163.18	GFO	17.27	S	5	953	42	63
200002142014	61.48	329.98	GFO	17.26	SE	3	951	30	79
199812241240	52.39	323.32	TOPEX	17.25	SSW	7	945	46	69
200303090245	48.04	333.45	TOPEX	17.25	SE	6	941	48	73
200305311653	-53.78	158.36	JASON1	17.22	NW	5.5	935	42	65
200001101009	62.16	338	GFO	17.17	SE	3.5	949	50	69
200308290052	-44.64	37.33	GFO	17.17	NW	10.5	941	38 (20 hr)	67
200709121742	-49.1	39.6	JASON1	17.04	NNE	7	933	30	63
200708291700	-51.71	85.83	ENVISAT	17.02	NNE	7	943	24	57
199403302134	53.64	338.91	TOPEX	16.99	SW	4	941	36	73
200803101142	48.98	351.97	ERS2	16.95	SW	4.25	943	28 (16 hr)	71
200410180131	22.5	128.16	TOPEX	16.94	TROPICAL				
199910050323	-55.4	25.59	TOPEX	16.94	NNE	6	925	38	57
199407201422	-53.55	31.13	TOPEX	16.89	N	8	939	22	57
199812281217	44.48	326.15	TOPEX	16.83	SW	3.5	965	28	77
200508262103	-37.5	20.85	ENVISAT	16.77	NW	15	957	24	61
200811270833	44.35	193.38	ENVISAT	16.76	SSE	4	949	30	65
200106241926	-59.16	27.39	TOPEX	16.74	NW	7	933	34	63
200807171928	-57.19	51.36	ENVISAT	16.69	NW	5	919	38	63
200304080333	-52.43	68.19	GFO	16.68	NW	7.5	943	40	67
199505282139	-53.88	44.83	TOPEX	16.68	NW	8	953	16*	59
199308100651	-48.94	124.81	TOPEX	16.68	NNW	4.5	937	24	59
200801020413	48.64	321.33	JASON1	16.66	SW	3.5	963	34	73
199804230945	-57.89	207.85	TOPEX	16.66	NW	10	941	26	65
200111051937	52.27	173.55	GFO	16.65	SSW	3.5	955	30	65
199412102348	46.56	169.4	ERS1	16.64	SSW	5.5	951	38	65
199912022339	44.37	195.84	TOPEX	16.63	SSE	7	961	40	73
200004190203	46.78	330.78	TOPEX	16.63	SW	2.5	965	28	71
200012310627	44.58	326.06	TOPEX	16.63	SSW	3.5	955	30	63
200201212331	42.23	328	TOPEX	16.63	SSE	4.5	961	32	73
199305240332	-47.94	95	ERS1	16.6	NW	8	951	34	63
200012020927	40.6	315.98	GFO	16.59	SSW	5.5	967	32	61
200302251934	48.26	320.23	GFO	16.59	SSE	5	961	20	55
200606140157	-44.06	246.79	GFO	16.59	NW	6	955	26	69
200104120348	-56.48	134.91	GFO	16.59	NNW	6	963	18	57
199507180750	-51.36	348.57	TOPEX	16.57	N	2	953	38	61
199512210712	39.4	185.54	TOPEX	16.57	SSW	4.8	947	50	77
199312112144	-57.11	178.19	ERS1	16.56	NW	2.5	941	34	65
200103311702	-56.36	162.76	GFO	16.54	NW	2	965	28 (20 hr)	65
199407011746	-46.75	80.03	ERS1	16.54	NW	4	959	30	61
199301212217	56.2	350.41	ERS1	16.53	SW	7.5	957	50	73
200611302143	63.33	346.93	ENVISAT	16.46	ENE	2	947	32	73
200110110533	44.44	190.11	TOPEX	16.43	SSE	1.5	959	38	69
199905171251	-61.06	41.25	TOPEX	16.43	NW	3	923	42	73
199910010340	-44.62	94.13	ERS2	16.41	NW	8.5	953	28	57
200201010923	-24.65	191.35	GFO	16.38	TROPICAL				
199903230029	41.33	157.92	ERS2	16.37	SSE	4.5	965	38	65
200112240711	44.93	188.31	GFO	16.37	SSE	7	939	36	63
200910151337	52.94	317.11	ENVISAT	16.33	SE	3.5	957	36	63
200808312059	-42.03	23.05	ENVISAT	16.32	NW	9	943	22	68
199206060939	-55.33	0.25	ERS1	16.31	NNW	4.5	931	30	71
200910272257	45.77	161.16	JASON1	16.3	SE	2.8	953	38	73
199407011606	-47.41	105.38	ERS1	16.28	NNE	5	949	38	59
199502141328	49.32	325.53	ERS1	16.27	SSW	4	957	26	57
200905140123	-54.33	117.21	ENVISAT	16.26	NW	5	941	34	63
199501020739	40.26	179.25	TOPEX	16.25	SSW	7	949	30	61
200607021421	-49	84.07	GFO	16.25	NW	8	945	6*	57
200302220133	35.49	169.67	TOPEX	16.22	SSE	5	955	30	63
199909301631	-47.07	190.73	TOPEX	16.22	NW	20	945	15 *	48
200103221458	-63.43	195.29	GFO	16.22	NW	8	945	26	61
200701011522	45.9	316.36	JASON1	16.2	SE	1	969	30	69
200205240919	-39.99	10.23	ERS2	16.19	NW	2.5	963	32	75
200605040630	-47.45	137.32	GFO	16.18	NW	7	947	22	69
199407290222	-59.4	90.32	TOPEX	16.15	NNE	3.5	945	36	55
200606231638	-50.48	91.02	ENVISAT	16.14	NW	9	931	40	61
200106232057	-59.03	7.24	TOPEX	16.12	NW	6	933	34	63
199910201517	46.62	327.79	TOPEX	16.12	SE	4.5	941	32	83
199711290524	55.72	182.19	TOPEX	16.1	SSW	3.5	951	30	67
199802190942	39.93	184.87	ERS2	16.08	SSW	6	957	36	67
199211041726	15.89	136.97	TOPEX	16.04	TROPICAL				
199405242202	-45.86	99.56	TOPEX	16.04	NW	7	961	20	55
200509011749	-53.91	74.69	ENVISAT	16.03	NW	5.5	945	12*	55
200510210742	47.6	206.85	JASON1	16.02	SW	5.5	961	22	59
200001071810	53.52	330.97	GFO	16.02	SW	9	949	28	61
200003101506	-62.3	170.39	TOPEX	16.02	NW	4	947	38	55
200005152203	-52.71	244.93	TOPEX	16.02	NW	3	941	31	66
199407192214	-49.89	14.15	ERS1	16	NW	4.5	953	18	61
199602161222	59.12	346.48	ERS1	16	SW	5	981	14	63

***The VESS associated with these peaks can be attributed more to a large pressure difference between the low center and a strong high pressure system, rather than a large deepening rate of the storm itself.**

The study plan is to eventually reanalyze the wind field and hindcast all of the 116 ETCs noted above. To date, a few of the highest ranked events have been addressed beginning with the events that occurred within the QuikSCAT period. Figure 7 shows typical continuity analyses of the track and time evolution of the central pressure in the ETC center and of peak wind speed in the core of the primary surface wind jet streak accompanying the ETC and associated with the generation of the VESS. The NAO examples are for the back-back systems that crossed the NAO during the first half of February, 2007. The NPO example is for the highest ranked VESS sampled in that basin within the QuikSCAT mission and the SIO example is rather typical of SIO VESS storms. While the evolution of the storm track and central pressure (and hence deepening rate) on these plots are from a detailed reanalysis, we find that in comparing these properties with those gleaned from the CFSR and the weather maps produced by the Ocean Prediction Center (OPC) of NOAA for the NAO and NPO storms and the Bureau of Meteorology of Australia we find generally good agreement. However, the CFSR surface wind fields tend to underspecify the peak wind speeds as the storm approaches and attains its peak and to lose continuity in the tracking of the core of the jet streak (see also Cox *et al*., 2011). Table 5 displays a preliminary summary of key storm properties as averages over the highest ranked VESS storms, based on the admittedly small sample reanalyzed to date, sorted by NAO, NPO and SIO. In addition to the minimum central pressure and deepening rate, this table also gives also the kinematically reanalyzed peak wind speed (equivalent 30-minute average at 10-meter elevation) and the average minimum distance between the speed max in the jet streak and the pressure center (Rmax). This minimum tends to occur near the time of occurrence of maximum storm intensity, as indicated in the continuity analyses of Figure 7. The reanalyses completed to data suggest the following preliminary conceptual model of the evolution of a "winter hurricane" capable of generating VESS of HS > 16 m.

Table 5

Preliminary estimates of average associated meteorological properties of minimum central pressure and maximum wind speed and its distance to the storm center for the highest ranked VESS storms in the NAO, NPO and SIO basins.

Basin	Min SLP (Mb)	Max Deepening Rate (mb/24 hrs)	Max Deepening Rate (Bergerons) @ 45N	Max Surface Wind Speed (m/s)	Min Radius of Max Winds (Km/deg)
North Atlantic	955	34	1.7	41	225/2
North Pacific	953	33	1.7	36	263/2.4
South Indian	945	29	1.5	34	4263.9

Stage I – Duration 12-24 hours: This marks the inception of the baroclinic instability that is to cause the rapidly intensifying ETC. The surface wind field is poorly organized with maximum winds in the 10-20 m/s range located typically 3-5 degrees equator-ward of the pressure center. The initial peak sea state is at a "background" level dependent mainly on precedent forcing.

Stage II – Duration ~ 24 hours: This marks the "explosive deepening" of the parent ETC. ETC of this class were first described by Sanders and Gyakum (1980) who defined such rapid intensification as a fall of central pressure of at least one Bergeron (defined as a pressure drop of at least 1 mb/hour maintained over at least 24 consecutive hours referenced to 60 deg latitude). The VESS "bombs" intensify more typically at a rate of 1.5 Bergerons (at 45 deg latitude, a deepening of 33 mb in 24 hours corresponds to 1.5 Bergerons). The radius of maximum wind in the right or right rear quadrant of the storm migrates

inward to within ~2 degrees of the pressure center in NAO and NPO storms (2-4 degrees in SIO storms) as the peak wind speed increases to super-Beaufort speeds (> 33 m/s) with 40 m/s not unusual especially in NAO and NPO. There is rapid growth of peak VESS from its background level to HS > 12 m in the vicinity of the jet streak maximum. The storm translation speed tends to lie between 15 m/s – 20 m/s.

Stage III - Duration ~ 12 hours: This is a fairly brief quasi- equilibrium stage of maximum intensity with respect to minimum central pressure, magnitude and location of maximum wind speed but with slow continued increase in peak VESS to its storm peak value.

Stage IV - Duration 24-48 hours: This marks the decay stage within which the central pressure rises rapidly, the peak wind speed and peak sea states decrease rapidly and the radius of maximum wind speed increases gradually as the overall storm circulation expands.

4. HINDCAST OF FEBRUARY 2007 NORTH ATLANTIC DUAL WINTER HURRICANES

On February 10th 2007 at 11:08 UTC, the GFO Ku band altimeter measured (unsmoothed) a HS of 20.24 m in the NAO at 48.14N 32.65W. This is the highest NAO HS in the GlobWave record analyzed in this study and close to highest HS overall (which is the TOPEX peak HS of 20.63 m in the central NPO storm of March 18, 1999). This peak occurred in the second of two very intense ETC to cross the NAO within one week during the first half of February 2007. The lead system, in fact, produced a peak HS of 19.15 m on February 9, 2007 at 21:31 UTC, this time estimated from JASON-1 Ku band altimeter (the C-band altimeter returned 20.2 m) 48.3N 19.2W. This was the highest significant wave height observed in the data set screened in C09. C09 also reported a hindcast of this lead storm made with our variant of a 3G wave model (Khandekar *et al.*, 1994) adapted to the NAO on a 30-minute grid.

The two storms were highlighted in the Mariners Weather Log review of NAO storms for the month as the lead storm was well monitored by QuikSCAT and it was claimed that wind speeds equivalent to Category 3 hurricane strength (Bancroft, 2007) were measured. A second storm following on the heels of the first storm was also monitored by QuikSCAT near its peak and again wind speeds of about 95 knots were also measured but over a much smaller area than in the first storm. As noted in C09, these QuikSCAT wind speeds were from the data set that used the so-called QSCAT-1/F13 model function used to derive ocean wind vectors from backscatter measurements at NASA/JPL/Pasadena, CA (QuikSCAT Science Data Product User's Manual). This model function replaced the QSCAT-1 model function developed during the mission validation/calibration phase and used for the standard so-called Level 2B processing of mission data between May 2, 2000 and the time of the switch to QSCAT-1/F13 in June, 2006. Since Level 2B data are not available post June 2006, C09 describe a linear regression that recovers the equivalent of QSCAT-1 wind speeds from QSCAT-1/F13 wind speeds. The model functions yield essentially identical wind speeds up to about 16 m/s while the QSCAT-1/F13 wind speeds are greater than the QSCAT-1 winds above 16 m/s and increasingly so at higher and higher wind speeds. Differences in the retrieval of wind direction between the two algorithms appear to be slight. According to the applied regression an F/13 wind speed of 30 m/s is adjusted to 27.2 m/s. An F/13 wind speed of 49 m/s, corresponding to 95 knots, the peak F/13 wind speed sensed by the QuikSCAT scatterometer in the two storms of early February 2007, is adjusted to ~83 knots (43 m/s). Of course, this simple linear regression cannot account for any relative differences between QSCAT-1 and QSCAT-1/F13 as a function of incidence angle and beam polarization, but at least the major source of bias in the F/13 wind speeds has been addressed and minimized.

Following the wind field kinematic reanalysis methodology described in more detail in C09, the wind fields surrounding the two migratory ETC were reanalyzed at 3-hourly intervals following the derivation of a detailed continuity analysis of the time and space evolution of the dominant jet streaks. It was found that both storms evolved closely in accordance to the conceptual model described above. Unlike the

hindcast in C09, which was based on NCEP/NCAR Reanalysis project background winds, the new hindcast not only covered both events in a continuous hindcast of the first half of the month but also assimilated the kinematic reanalyses into the CFSR background winds. The lead ETC formed south of Nova Scotia on February 8th and moved northeastward across the NAO attaining its maximum intensity (minimum central pressure) of 952 mb near 50 N, 30 W at 0600 UTC February 9th, which is about 15 hours prior to the JASON-1 pass that sampled the peak VESS. Over the 24-hour period preceding the time of minimum pressure, the central pressure fell from 988 mb to 952 mb, a deepening of 36 mb/24 hours corresponding to a rate of nearly 1.7 Bergerons. The average forward speed of the cyclone was close to 25 knots. This storm was very well monitored by QuikSCAT, which measured an "adjusted" (as described in more detail above) peak wind speed of 83 knots, and an apparent duration of peak wind speeds above 50 knots of at least 36-hours. The following ETC also formed in the vicinity of Nova Scotia at about 1200 UTC on February 8th and deepened to 964 mb by 1200 UTC February 10th, with a maximum analyzed deepening rate of 32 mb/24 hours. A QuikSCAT pass observed the entire core of the storm at around the 2100 UTC February 9th pass and as with the lead storm measured peak wind speeds (as adjusted to equivalent QSCAT-1) of about 83 knots. The QuikSCAT passes at the time of maximum intensity of both storms indicate that by the time of peak intensity the radius of maximum wind has contracted to about 90 Nm, still larger than is typical for a tropical cyclone but much smaller than typically specified by even the best reanalysis products.

The wave hindcast was executed on the same grid system and using the same wave model physics used for the MSC50 hindcast (Swail *et al*, 2006), namely a grid of average 30 nm spacing running Oceanweather's standard 3G physics (Khandekar *et al*, 1994; Forristall and Greenwood, 1998). The envelope of the peak HS response is shown for each event in Figure 8. Note the area of 20 m HS that develops on the eastern edge of the area where wind speeds peaked, but this wave response is maintained eastward aided by propagation effects, even as the peak modeled wind speed decreases gradually. These plots suggest strongly that the peak VESS HS in these two storms was essentially captured by the JASON-1 and GFO passes. Figure 8 also shows the envelope of the peak hindcast wind speed and the peak hindcast HS for the combined run. The wind speed envelope plot shows that the two separate jet streaks evolving with that of the lead system further east. The maximum overall peak hindcast HS was associated with the lead storm at 21.1 m. In C09, the second storm was not detected and it was assumed that only one pass viewed the lead system. Using GlobWave there are four altimeter cuts through the core of the lead storm and three altimeter cuts through the following system. Figure 9 compares the hindcast with the altimeter measurements for the GFO orbit segment through the peak of the second system (a similar comparison is made for the lead system in C09) for a run made with pure CFSR wind forcing and the run made with the kinematically reanalyzed wind speeds. More often than not CFSR forcing leads to the pattern seen here; that is, the hindcast is very skillful overall but there is a trend to miss the peak sea state by several meters (see also Cox *et al*., 2011), whereas (based on our on-going program to hindcast all 120 extreme VESS storms) a careful continuity analysis of the evolution of the dominant surface wind jet streaks in each system followed by kinematic reanalysis allows the resolution of the storm VESS peak with negligible bias, at least where the reanalysis is aided by the QuikSCAT dataset.

5. SUMMARY AND CONCLUSIONS

1. The new GlobWave database of global satellite altimeter estimates of wind speed and wave height from seven missions spanning the period August, 1991 – March, 2010 was scanned, filtered and distilled using automated and man-machine mix procedures to yield over 5000 basin specific orbit segments with peak HS > 12 m, which were subsequently distilled to a population 120 individual storms in which there was at least one altimeter estimate of HS > 16 m (extreme VESS!).

2. The highest HS were observed in the NH with ten (four) orbits segments in the NAO (NPO) with a peak HS of > 18 m. Three HS peaks > 18 m were seen in the Southern Oceans. Only three of the > 5000

orbit segments identified has a peak HS greater than 20 m and none was greater than 20.6 m. These estimates are based on a scan of the database at the intrinsic sampling rate (generally 1 Hz). Smoothing or median filtering the data stream over ~ a 50 km orbit length reduces the peaks on average by about 0.9 m.

3. The number of VESS storms detected was found not to be proportional to basin size but rather the frequency of storms was found to be greatest in the NAO (the smallest basin) followed by the NPO, SIO, SPO and SAO. This appears to be consistent with general circulation studies of extratropical cyclogenesis, frequency and intensity in general atmospheric circulation models. For example, Brayshaw *et al*. (2009) found that North America has the ideal shape to enhance land-sea contrast and strength of baroclinicity leading to robust generation of intense cyclone over the North Atlantic basin as it provides an environment especially conducive to strong baroclinic instability.

4. The detection rate of extreme VESS storms using the methods applied in this study, at about 5 events per year on a global basis, appears to be insensitive to the number of simultaneous missions as long as there are at least two.

5. All but four of the 120 extreme VESS storms (i.e. with HS > 16 m) detected were associated with extratropical cyclones. This reflects mainly the poor sampling of the small area of sea states in the inner core of tropical cyclones by satellite mounted small-footprint nadir pointing altimeters rather than any intrinsic reluctance of intense tropical cyclones to excite VESS.

6. Peak wind speeds (equivalent neutral wind speed at 10-m elevation) in the most intense VESS storms exceed 40 m/s, a speed which transforms using a prevalent gust model to a peak sustained 1-minute wind speed (the reference interval used to classify hurricanes) of about 100 knots or 115 mph. This speed corresponds to a hurricane of Saffir-Simpson Category 3, though the scale of the wind field and the radius of maximum wind speed of these ETC events are much greater than typical of an intense tropical cyclone. The terms “Hurricane Force Extratropical Cyclones” (HFEC) and “Winter Hurricanes” have been used to describe mid-latitude winter storms with hurricane wind speeds (e.g. Von Ahn *et al*., 2006; Businger, 2011).

7. A 3G wave model hindcast of a stormy two-week period in the NAO during February, 2007 within which the two highest ranked VESS events in that basin were detected was found to be in close agreement with the total of seven orbit segments with peak HS > 12 m that transected these two events. As concluded also in C09, this agreement provides tentative evidence that a proven 3G model may be applied to hindcast VESS in severe “HFEC’ with confidence as long as the forcing is accurately prescribed, at least with respect to specification of HS. It will be extremely challenging of both models and measurement systems to be able to extend this confidence to accurate specification of the full 2D spectrum associated with VESS.

REFERENCES

Ash, E. D. Carter and F. Collard, 2011: DUE GlobWave Wave Data Handbook, Sept, 2001. Logica, UK Ltd.58pp.
http://www.globwave.org/content/download/10362/68974/file/GlobWave_D.9_WDH_v1.0.pdf

Bancroft, G. P., 2007: Marine Weather Review – North Atlantic Area January through April, 2007. Mariners Weather Log, 51, 38-53.

Brayshaw, D. J., B. Hoskins, and M. Blackburn, 2009: The basic ingredients of the north Atlantic storm track. Part 1: land-sea contrast and orographt. J. Atmos. Sci., 66:2539-2559.

Buchner, B., G. Forristall, K. Ewans, M. Christou and J. Hennig, 2011: New insights in extreme crest height distributions (A summary of the CREST JIP. OMAE 2011-49846, June 19-24, Rotterdam,The Netherlands.

Businger, S. 2011: Impact of hurricane force wind fields on the North Pacific Ocean Environment. 12th International Workshop on Waves and Coastal Hazards, October 31-November 4, Kona, Hawaii.

Cardone, V. J., R. E. Jensen, D. T. Resio, V. R. Swail and A. T. Cox, 1996. Evaluation of contemporary ocean wave models in rare extreme events: Halloween storm of October, 1991; Storm of the century of March, 1993. J. of Atmos. And Ocean. Tech., 13, 198-230.

Cardone V.J., A.T. Cox, E.L. Harris, E.A. Orelup, M.J. Parsons and H.C. Graber. Impact of QuikSCAT Surface Marine Winds on Wave Hindcasting. 8th International Wind and Wave Workshop, Oahu, Hawaii November 14-19, 2004.

Cardone, V. J., A.T. Cox, M. A. Morrone and V. R. Swail, 2009: Satellite altimeter detection of very extreme sea states (VESS). 11th International Workshop on Wave Hindcasting and Coastal Hazards. Halifax, NS.

Cardone, V.J., A.T. Cox and G.Z. Forristall, 2007: OTC 18652: Hindcast of Winds, Waves and Currents in Northern Gulf of Mexico in Hurricanes Katrina (2005) and Rita (2005). 2007 Offshore Technology Conference, May 2007, Houston, TX.

Cardone, V. J. and A.T. Cox, 2011: Modeling very extreme sea states (VESS) in real and synthetic design level storms. OMAE 2011-49731, June 19-24, Rotterdam, The Netherlands.

Chao, Y. Y. and H. Tolman, 2010: Performance of NCEP regional wave models in predicting peak sea states during the 2005 North Atlantic hurricane season. Wea. & Forecasting, 25, 1543-1567.

Cox, A. T., J. A. Greenwood, V. J. Cardone, and V. R. Swail, 1995: An interactive objective kinematic analysis system. Proceedings of the 4th International Workshop on Wave Hindcasting and Forecasting, October 16-20, 1995. Banff, Alberta, Canada, p. 109-118.

Cox, A. T. and V. J. Cardone, 2011: On the Use of the Climate Forecast System Reanalysis Wind Forcing In Ocean Response Modeling. 12th International Workshop on Wave Hindcasting and Coastal Hazards. October 31 – November 4, Kona, Hawaii.

Forristall, G.Z. and J. A. Greenwood, 1998. Directional spreading of measured and hindcasted wave spectra. Proc. 5th International Workshop on Wave Hindcasting and Forecasting, Melbourne, FL, January 26-30, 1998

Garrett, C. and J. Gemmrich2009. Rogue Waves. Physics Today, American Institute of Physics, June 2009

Holliday, N. P., M. J. Yelland, R. Pascal, V. R. Swail, P. K. Taylor, C. R. Griffiths, and E. Kent (2006), Were extreme waves in the Rockall Trough the largest ever recorded?, Geophys. Res. Lett., 33, L05613, doi:10.1029/2005GL025238.

Jensen, R.E., V.J. Cardone and A.T. Cox, 2006: Performance of Third Generation Wave Models in Extreme Hurricanes. 9th International Wind and Wave Workshop, September 25-29, 2006, Victoria, B.C.

Khandekar, M. L., R. Lalbeharry and V. J. Cardone. 1994. The performance of the Canadian spectral ocean wave model (CSOWM) during the Grand Banks ERS-1 SAR wave spectra validation experiment. Atmosphere-Oceans, 32, 31-60.

Powell, M. D., S. Murillo, P. Dodge, E. Uhlhorn, J. Gamache, V. Cardone, A. Cox, S. Otero, N. Carrasco, B. Annane and R. St. Fleur, 2008. Reconstruction of Hurricane Katrina's Wind field for Storm Surge and Wave Hindcasting. Ocean Engineering (in print)

Queffeulou, P. and D. Croize-Fillon, 2010: Global altimeter SWH data set – May, 2010. IFRMER, Plouzane France.

QuikSCAT Science Data Product User's Manual. Overview & Geophysical Data Products. Version 3.0. Sept. 2006, D-1805-Rev A.

Rosenthal, W. and S. Lehner, 2008: Rogue waves: results of the MaxWave Project. J. Offshore Mech. Arct. Eng., 130, Issue 2, 8 pp.

Saha, Suranjana, Shrinivas Moorthi, Hua-Lu Pan, Xingren Wu, Jiande Wang, Sudhir Nadiga, Patrick Tripp, Robert Kistler, John Woollen, David Behringer, Haixia Liu, Diane Stokes, Robert Grumbine, George Gayno, Jun Wang, Yu-Tai Hou, Hui-ya Chuang, Hann-Ming H. Juang, Joe Sela, Mark Iredell, Russ Treadon, Daryl Kleist, Paul Van Delst, Dennis Keyser, John Derber, Michael Ek, Jesse Meng, Helin Wei, Rongqian Yang, Stephen Lord, Huug van den Dool, Arun Kumar, Wanqiu Wang, Craig Long, Muthuvel Chelliah, Yan Xue, Boyin Huang, Jae-Kyung Schemm, Wesley Ebisuzaki, Roger Lin, Pingping Xie, Mingyue Chen, Shuntai Zhou, Wayne Higgins, Cheng-Zhi Zou, Quanhua Liu, Yong Chen, Yong Han, Lidia Cucurull, Richard W. Reynolds, Glenn Rutledge, and Mitch Goldberg, 2010: The NCEP Climate Forecast System Reanalysis. Bull. of AMS, August 2010, 1015-1057.

Sanders, F. and J. R. Gyakum, 1980: Synoptic-dynamic climatology of the "Bomb". Mon. Wea. Rev, 108, 1589-1606.

Soares and Swail, 2006. The WMO/IOC JCOMM Wave Programme. 9th International Wind and Wave Workshop, Victoria, B.C. Sept. 25-29, 2006.

Swail, V.R., V.J. Cardone, M. Ferguson, D.J. Gummer, E.L. Harris, E.A. Orelup and A.T. Cox, 2006 The MSC50 Wind and Wave Reanalysis. 9th International Wind and Wave Workshop, September 25-29, 2006, Victoria, B.C.

Thibaut, P F. Ferreira and P. Femenias: Sigma0 blooms in the ENVISAT radar altimeter-dat. Proc. ENVISAT Symposium 2007, Montreux, Switzerland, 23-27 April 2007. ESA SP-636, July, 2007.

Von Ahn, J.M., Sienkiewicz and P. Chang, 2006: Operational impact of QuikSCAT winds in the NOAA Ocean Prediction Center. Weather and Forecasting, 21,523-539.

Waseda, T, T. Kinoshita and H. Tamura, 2009: Evolution of a random directional wave and freak wave occurrence. J. Phy. Oceanog., 39, 621-639.

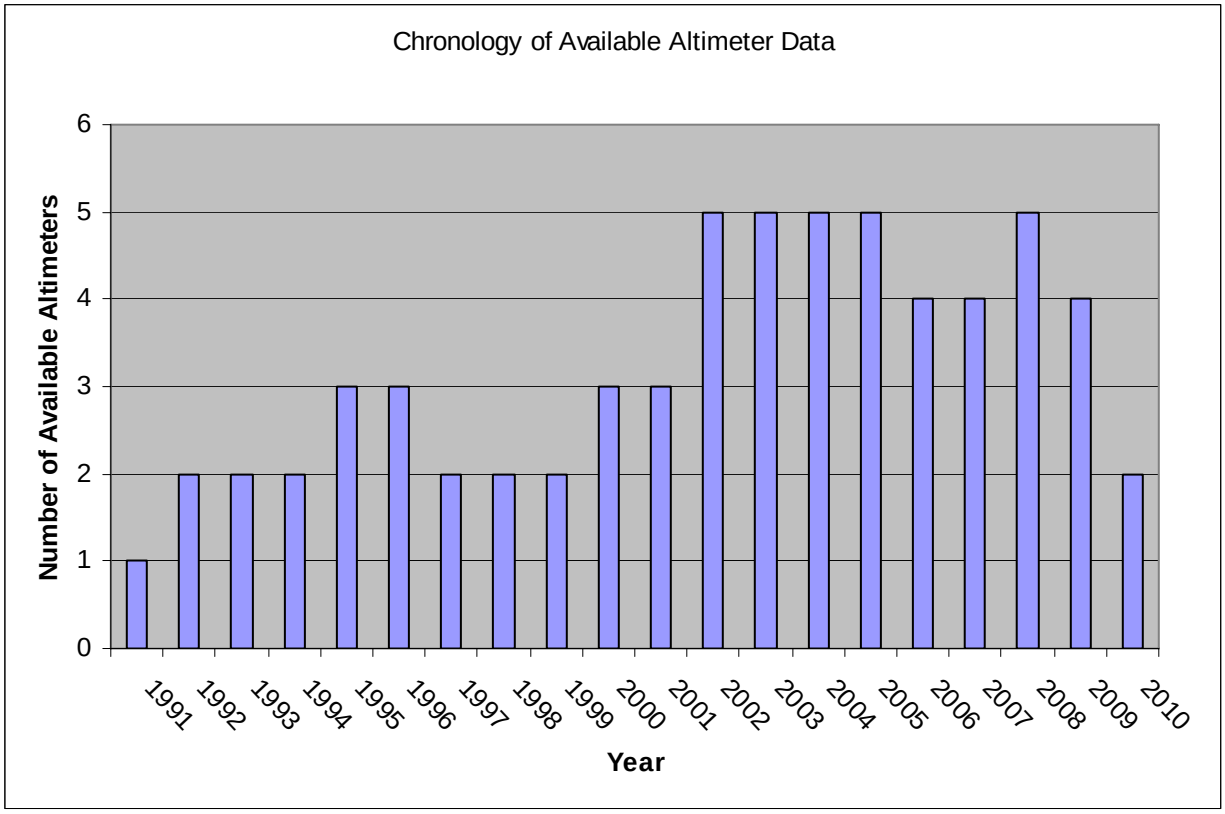

Figure 1 – Number of altimeter missions in GlobWave database by year

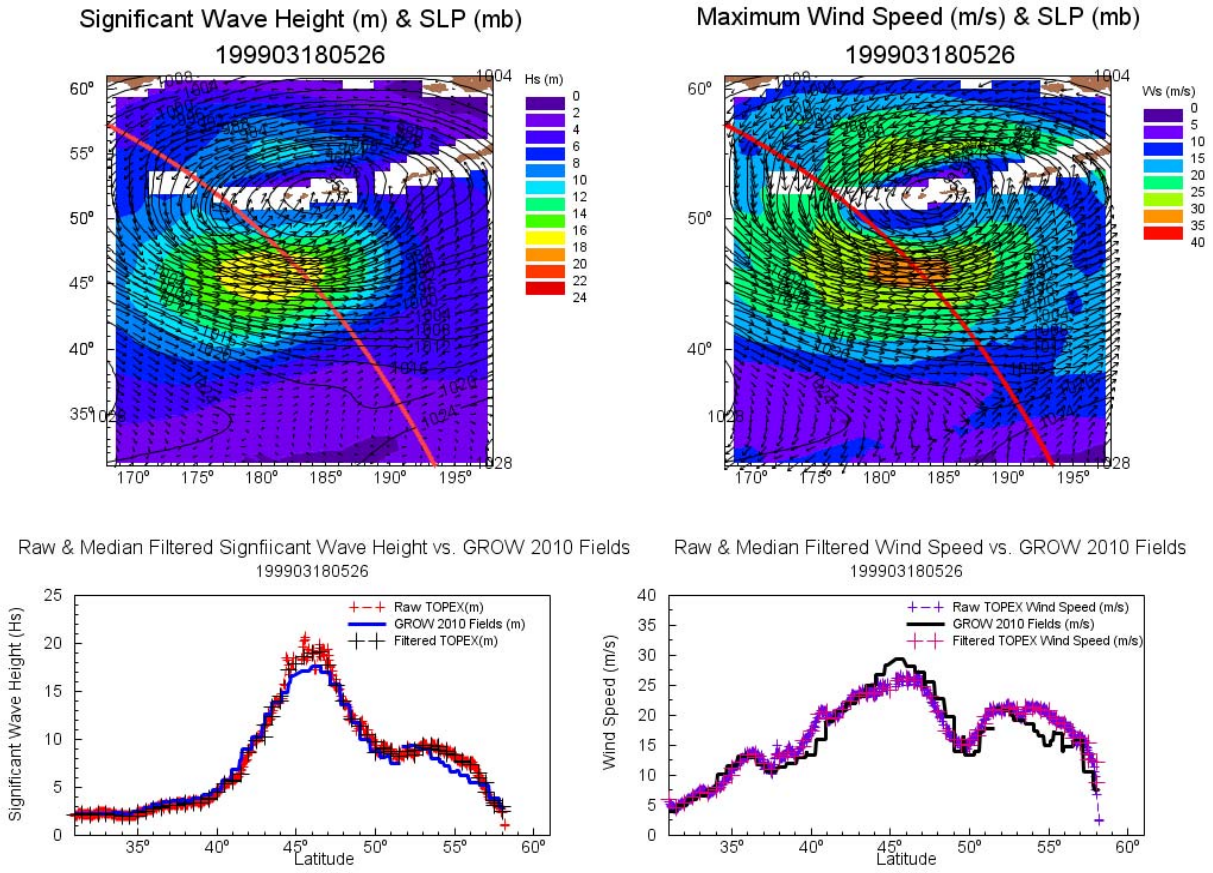

Figure 2 – Above, example plot of storm centered CFSR driven hindcast HS field (left) and surface wind field (right) superimposed on CFSR isobar analysis; below, TOPEX HS (left) and WS (right) storm transects (as plotted above), raw and filtered, compared to CFSR wind speed and CFSR based wave hindcast, for the North Pacific VESS peak of 199903180526 UTC wind speed and CFSR based wave hindcast, for the North Pacific VESS peak of 199903180526 UTC

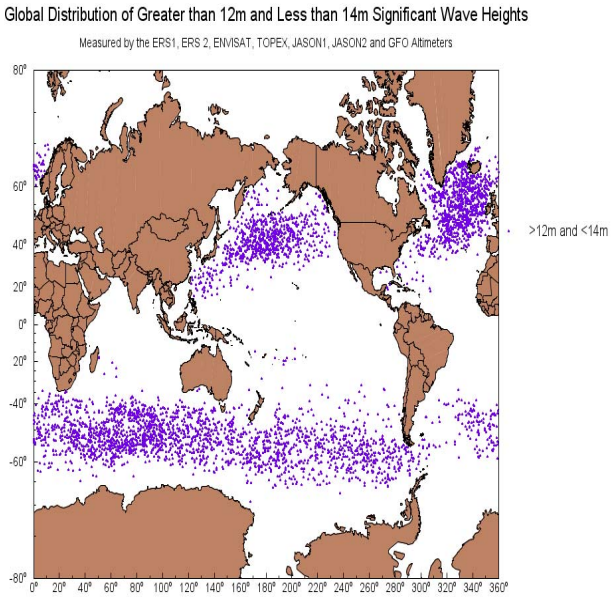

(a)

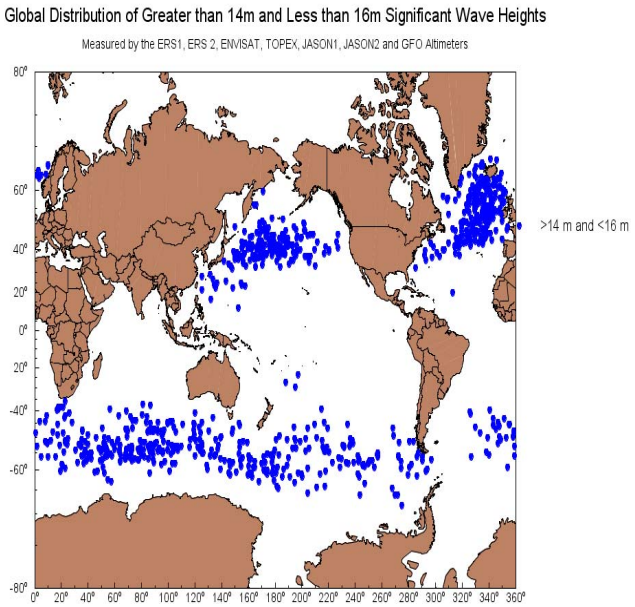

(b)

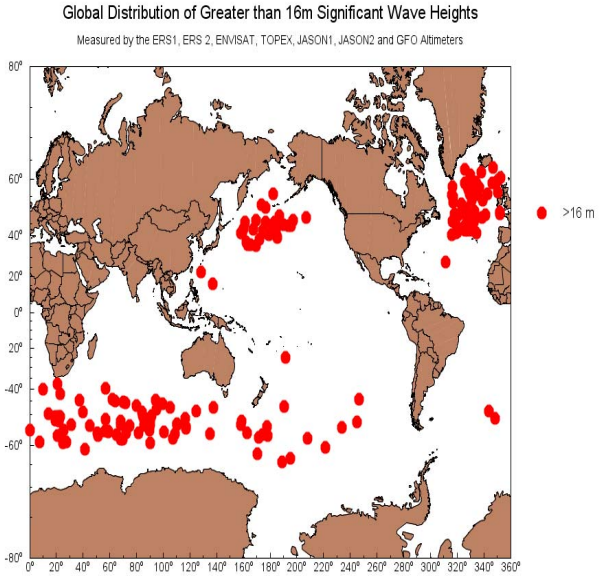

(c)

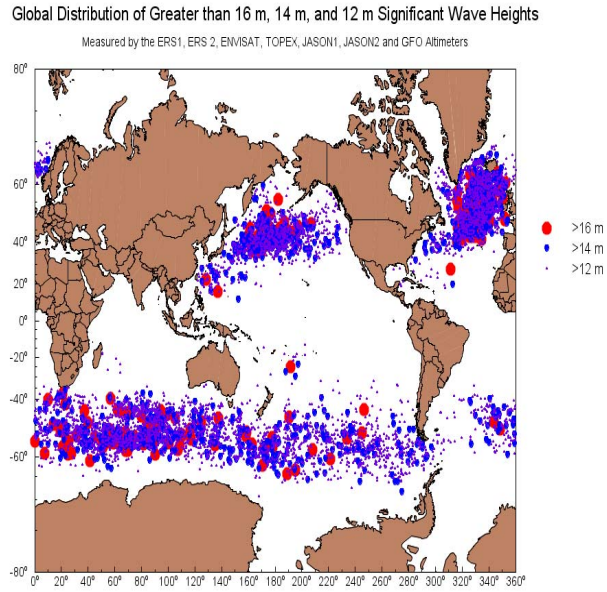

(d)

Figure 3 – Plots of global distribution of GlobWave HS basin specific orbit segment peaks: (a) 12-14 m, (b) 14-16 m, (c) > 16 m, (d) All Peaks

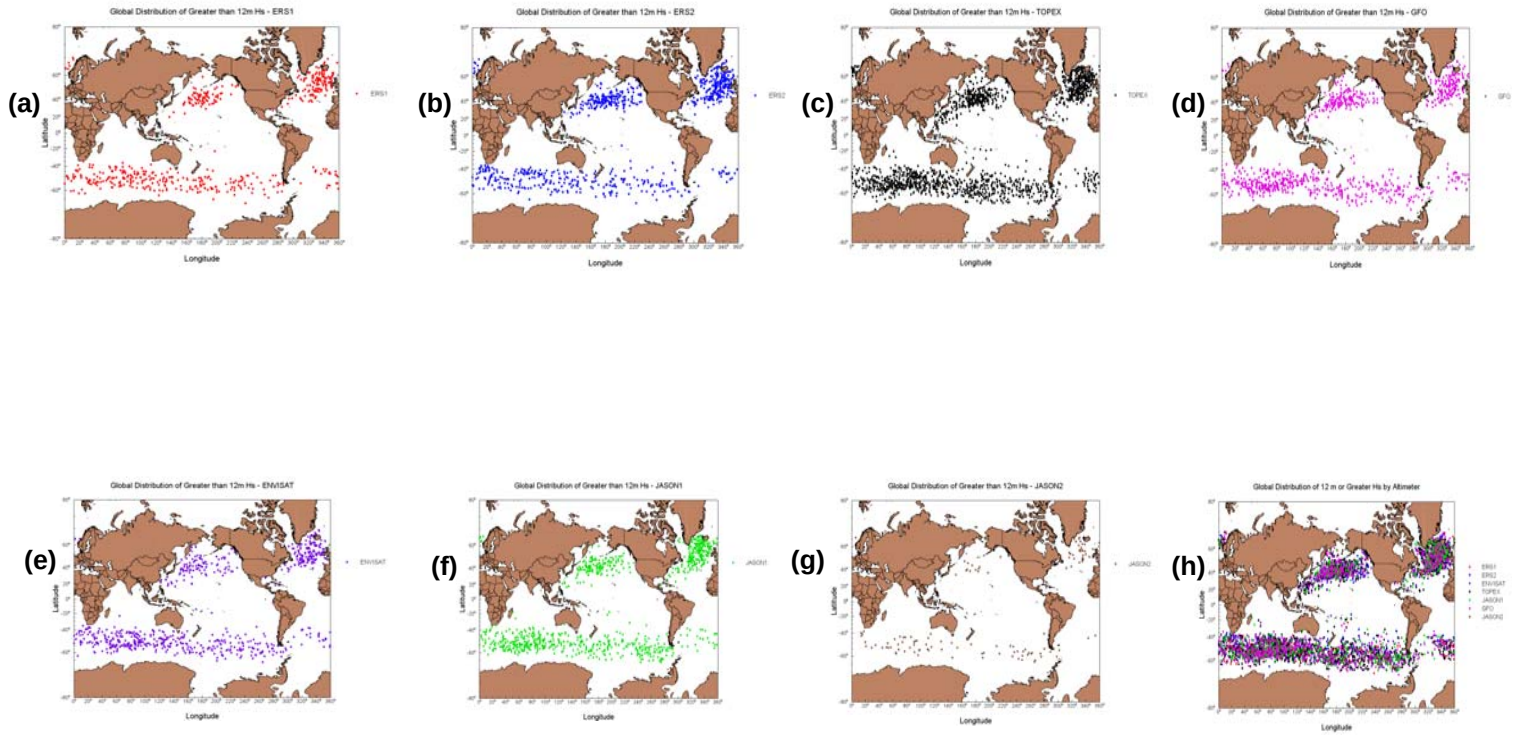

Figure 4 – Global distribution of HS > 12m in GlobWave database for (a) ERS1, (b) ERS2, (c) TOPEX, (d) GFO, (e) ENVISAT, (f) JASON1, (g) JASON2, and (h) all altimeters

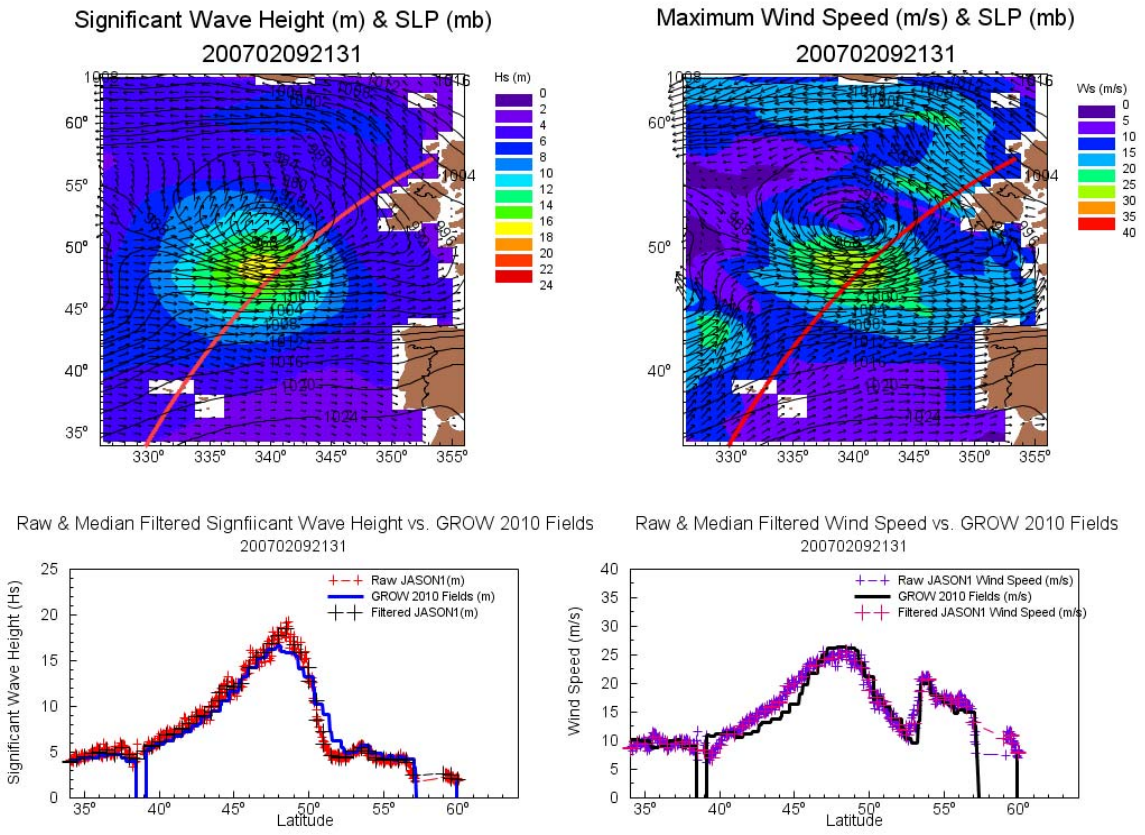

Figure 5 – Above, plot of storm centered CFSR driven hindcast HS field (left) and surface wind field (right) superimposed on CFSR isobar analysis; below, JASON1 HS (left) and WS (right) storm transects (as plotted above), raw and filtered, compared to CFSR wind speed and CFSR based wave hindcast, for the 2nd highest ranked VESS (19.15 M) North Atlantic storm of February 9, 2007

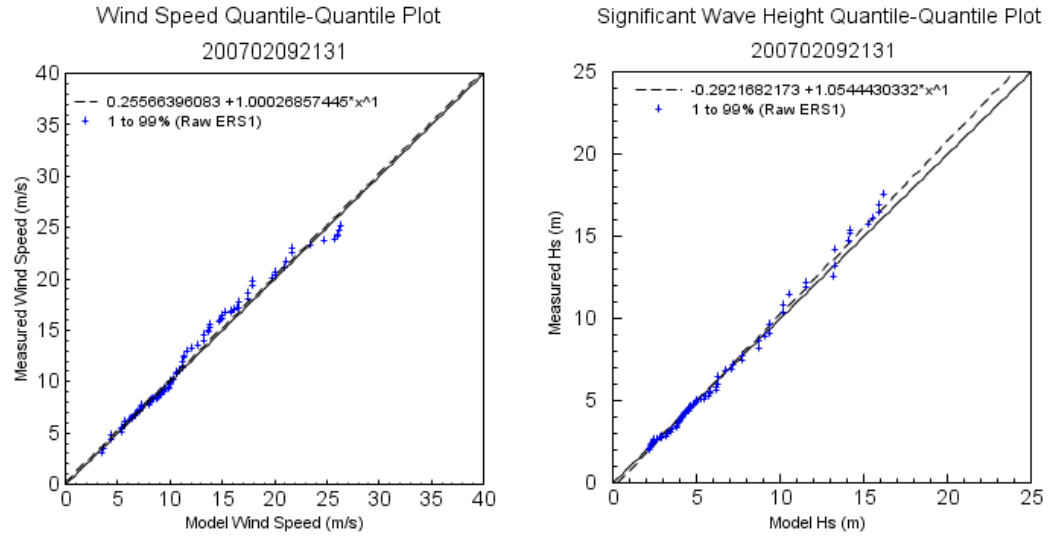

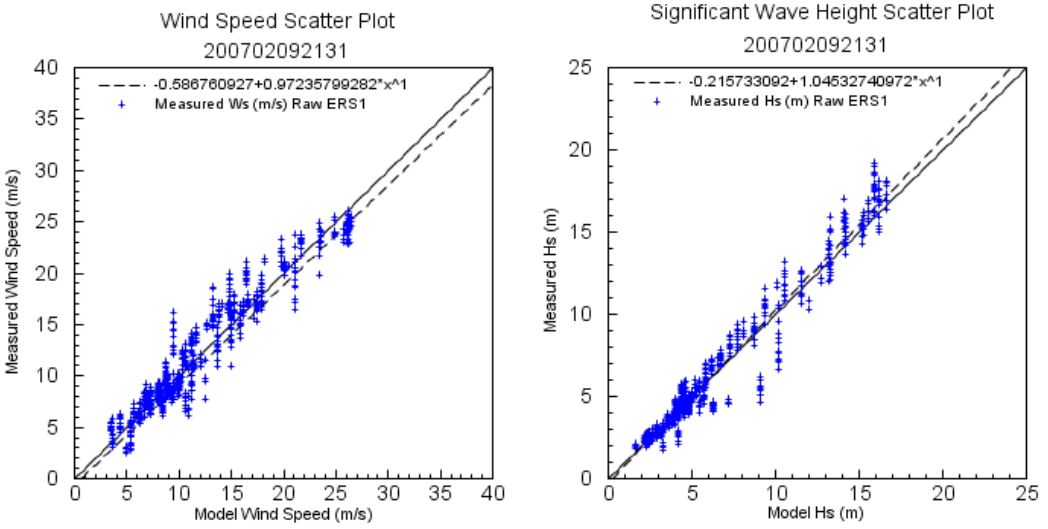

	Number of Pts	Mean Meas	Mean Hind	Diff (H-M)	RMS Error	Stnd Dev	Scat Index	Ratio	Corr Coeff
Wind Spd. (m/s)	821	12.29	12.04	-0.25	1.63	1.61	0.13	0.44	0.96
Sig Wave Ht (m)	821	5.92	5.87	-0.05	0.89	0.89	0.15	0.42	0.98

Figure 6: CFSR winds and driven hindcast qantile-quantile plot (above) and scatter plots and difference statistics (below) for HS (m) and WS (m/s) for the orbit segment shown

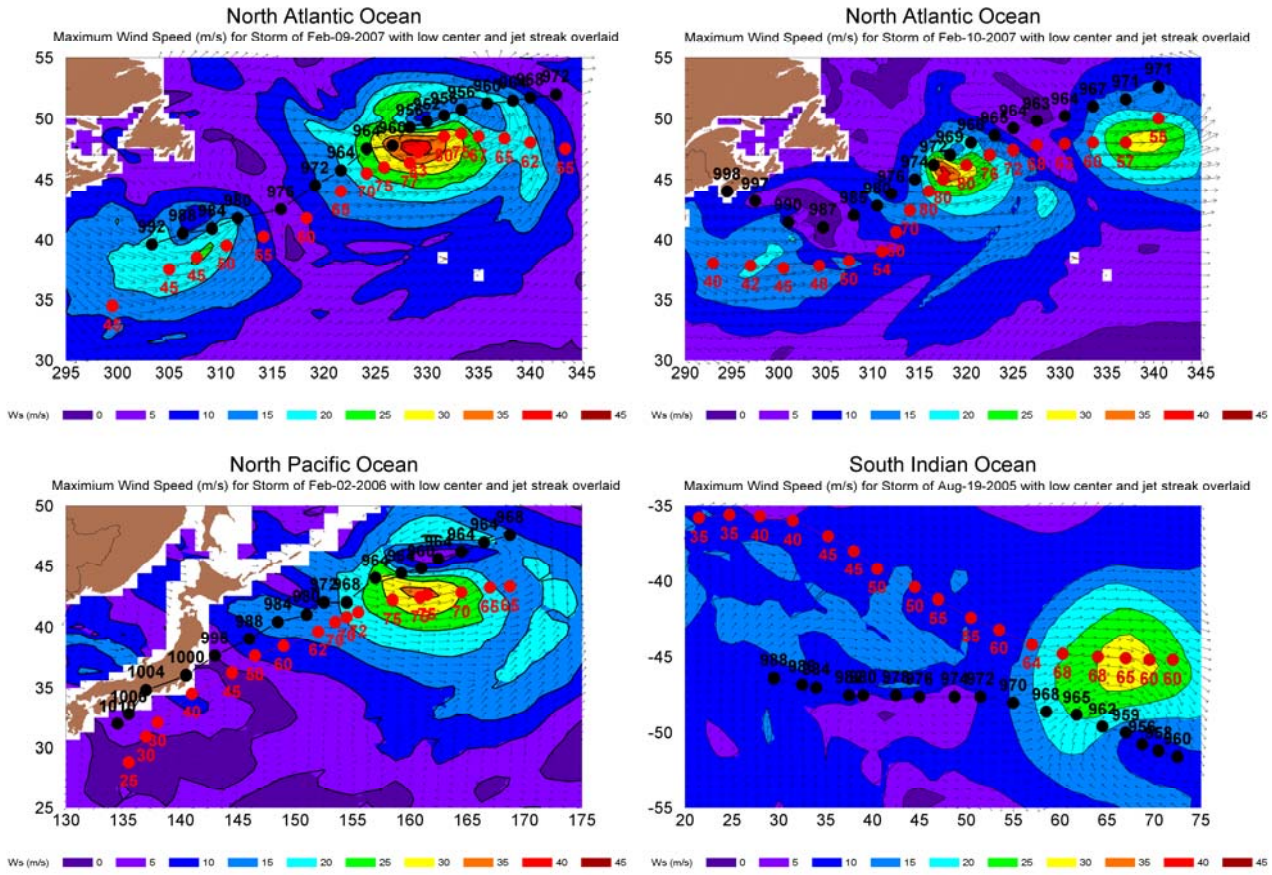

Figure 7. Kinematiclly reanalyzed continuity analysis at 3-hourly intervals of the track of storm pressure center (minimum pressure shown in mb) and the core of the main surface wind jet streak (peak wind speed shown in knots) in highest ranked example of storms in the North Atlantic 9 (above) , North Pacific (lower left) and South Indian Ocean (lower right)

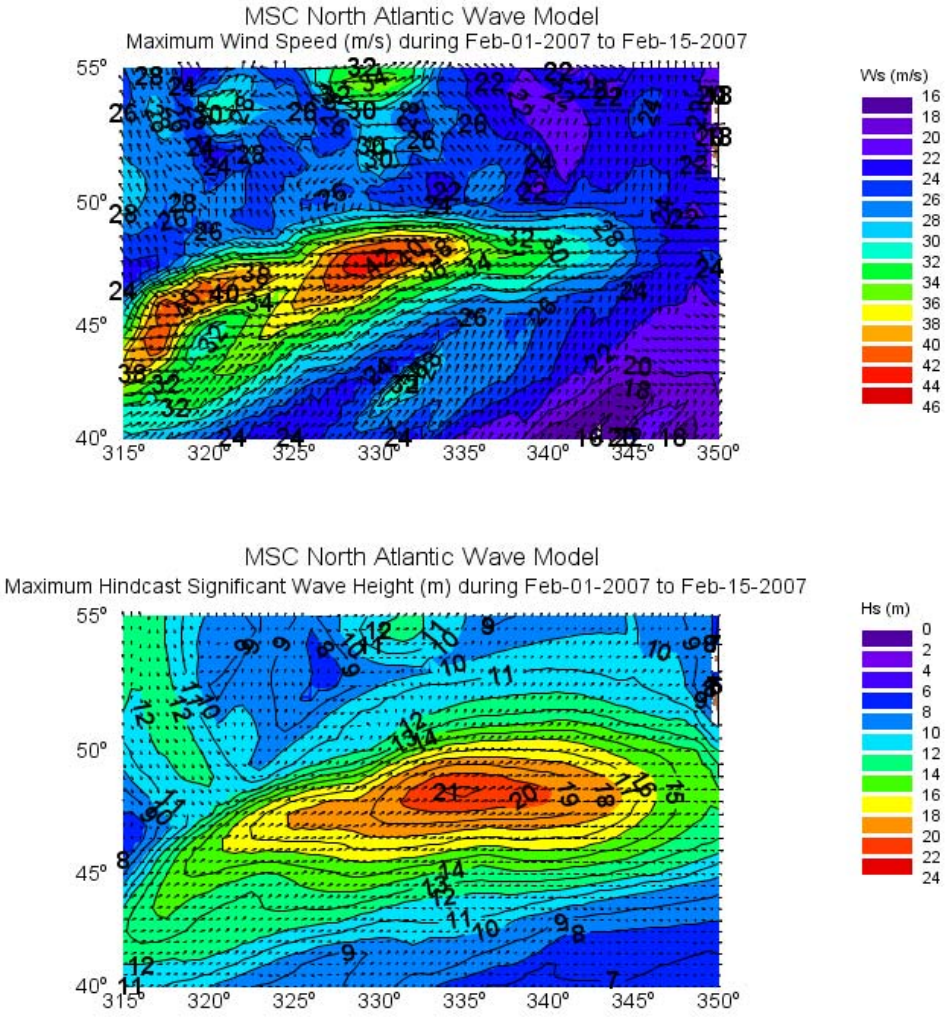

Figure 8: Envelope of maximum hindcast WS (above, m/s) and HS (below, m) over the period Feb 01-15, 2007 based on kinematically reanalyzed wind fields.

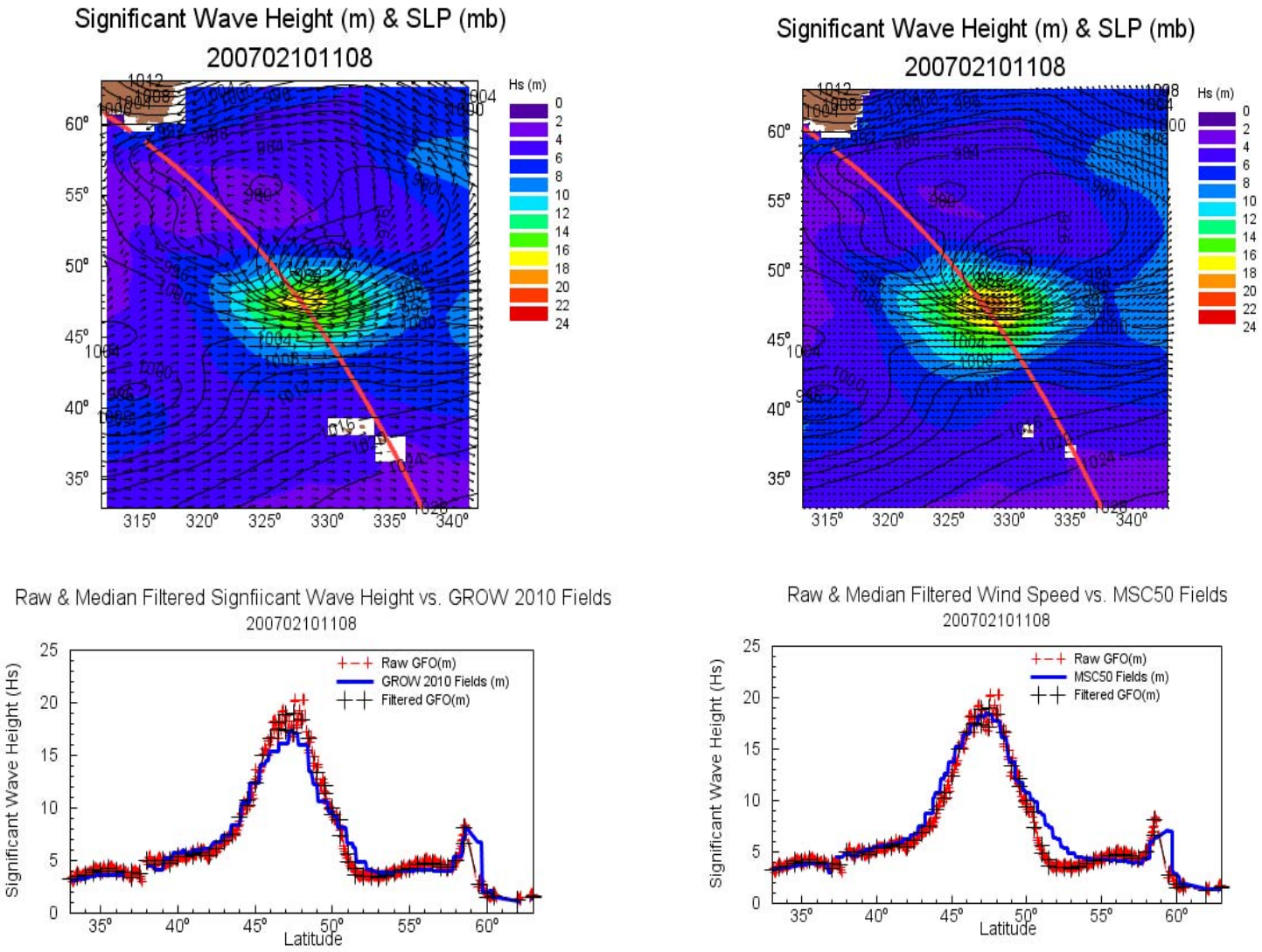

(a) **(b)**

Figure 9: Above: maximum hindcast HS (m) overlaid over CFSR SLP (mb) analysis for CFSR driven (GROW2010) hindcast (left) and hindcast (MSC50) driven by kinematically reanalyzed wind fields (right) with corresponding comparisons below between the hindcasts and the GFO orbit segment shown for the highest ranked NAO VESS of Feb-10-2007.